

Article

# Air Entrainment and Air Demand in the Spillway Tunnel at the Jinping-I Dam

Jijian Lian <sup>1</sup>, Chunfeng Qi <sup>1</sup>, Fang Liu <sup>1,\*</sup> , Wenjuan Gou <sup>1</sup>, Shunqi Pan <sup>2</sup>   
and Qunan Ouyang <sup>1</sup>

<sup>1</sup> State Key Laboratory of Hydraulic Engineering Simulation and Safety, School of Civil Engineering, Tianjin University, Tianjin 300072, China; tju\_luntan@126.com (J.L.); qcf\_2011@tju.edu.cn (C.Q.); gwj@tju.edu.cn (W.G.); oyqa@tju.edu.cn (Q.O.)

<sup>2</sup> School of Engineering, Cardiff University, Cardiff CF24 3AA, UK; PanS2@cardiff.ac.uk

\* Correspondence: fangliu@tju.edu.cn; Tel.: +86-135-1287-1269

Received: 3 August 2017; Accepted: 7 September 2017; Published: 10 September 2017

**Abstract:** Artificial air entrainment has been widely used to avoid cavitation damage in spillways where high-velocity flow occurs, and its performance is very important for spillway safety. In order to evaluate the performance of the aeration system in the spillway tunnel of the Jinping-I Dam, which is the highest arched dam in the world to date, systematic prototype observation was conducted. Ventilation characteristics of the air supply system and aeration-related characteristics of the aeration devices were examined at the prototype scale. The results showed that air flows smoothly in the air intake well and the real effect of air entrainment of the aeration device was desirable. In contrast with results from laboratory tests with a physical model at a scale of 1/30 following the gravity similarity, it was found that air demand in the prototype is much greater, clearly indicating the scale effect. By summing up and analyzing the air demand ratio of the prototype to the model in some projects, the scale effect was found to be ignorable when the model scale was greater than 1/10. In addition, based on a series of prototype data on air demand, a brief evaluation of present calculation methods for air demand was conducted and a new form of calculation method for air demand related to unit width flow rate was established. The present prototype results can be used as a reference for similar engineering design, and to validate and verify numerical simulations as well as model tests.

**Keywords:** air entrainment; prototype observation; air demand; cavitation noise; scale effect; Jinping-I Dam

## 1. Introduction

High-velocity flow often occurs on spillways, particularly for high dams, which can cause severe cavitation damage to the hydraulic structures. Some measures, such as optimizing the structure body, smoothing the concrete surface, and applying anti-cavitation materials are commonly implemented to prevent the cavitation, but the potential damage cannot be completely eliminated. Engineering experiences show that artificial air entrainment is an economical and effective way to protect the concrete surface from cavitation damage by means of setting auxiliary devices on the bottom of spillways and sometimes on sidewalls [1–5]. Aeration devices have been widely used in many projects since the successful application of a groove in the Great Coulee Dam in 1960 [6], and significant damage reduction has been achieved. Peterka [7] proposed that when the air concentration in the flow layers close to the channel bottom reaches 5–8%, the concrete surface can be completely protected from cavitation damage. Rasmussen [8], who conducted a number of surface erosion experiments with a variety of measuring instruments, confirmed that 0.8–1.0% volume of small air bubbles in the water flow could also effectively play a protective role to the concrete surface. Russell [9] suggested that the critical air concentration to avoid cavitation damage is 2.8%.

Research on air entrainment is mainly conducted through theoretical analysis, laboratory experiments, and prototype observations. Theoretical analysis on the mechanism of air entrainment mainly focuses on the occurrence of cavitation, and processes of air in-flow and out-flow. Many researchers (Ball [10], Hamilton [11], Wood [12], Elder [13], Falvey [14]) investigated the relationship between the critical cavitation number with surface irregularity, turbulent boundary layer thickness and flow velocity. Jet aeration is mainly caused by the turbulent exchange of air–water interface. It is generally believed that when the flow velocity exceeds 5–7 m/s, the upper surface of the flow begins to be aerated. However, for the lower surface, there exist different opinions on critical aeration from different researchers, such as those of Pan et al. [15], Pinto [5], Koschitzky and Kobus [16], Rutschmann and Hager [2], May et al. [17] and Chen and Yu [18]. In general, the law of single bubble motion in the water is the basis for understanding the aeration mechanism. Haberman and Morton [19] conducted an earlier study on the theory of single bubble motion in still water. Following this study, Comlet [20] considered the effects of resistance, gravity and buoyancy on bubble motion. Volkart [21], who compared the movement of bubbles in moving and still waters, found that rising velocity of bubbles in moving water is only 1/10 of that in still water. Although considerable work has been done, due to the complexity of air entrainment phenomenon, particularly for the spillways constructed in a tunnel, an accurate theoretical model is yet to be established. In laboratory experiments, the air entrainment phenomenon is known to be difficult to accurately model because of the unknown scale effects [22]. Traditional hydraulic model tests, generally designed based on the gravity similarity, may exclude the effects of viscosity and surface tension, so the turbulence intensity cannot be properly represented, whilst the air entrainment phenomenon is strongly related to flow turbulence intensity. The model scale required to accurately represent the turbulence-induced air demand is yet to be quantified.

Given the fact that mathematical models for air entrainment have not yet been well established and the traditional model tests are affected by the scale effect, prototype observations become important in the air entrainment research [23]. The information of air entrainment phenomenon can be obtained through directly monitoring the operating of hydraulic structures, and detailed prototype results can be used to verify and validate mathematical models and also evaluate laboratory experiments. Up to now, prototype observations on cavitation damage and the air entrainment phenomenon have been conducted on many projects. The Mica Dam in Canada was the first to be used to conduct prototype observations on air entrainment and the devices used proved to be successful in cavitation damage alleviation. Similar examples include the Glen Canyon Dam in the United States [24], Foz do Areia Dam in Brazil [5], Guri 2 Dam in Venezuela [25], Tarbela Dam in Pakistan [26], and the Bratsk Dam in the former Soviet Union [27], as well as the Fengjiashan Dam, Wujiangdu Dam [28], and Xiaowan Dam in China.

Jinping-I Dam, with its height of 305 m, is the highest arched dam in the world at present. Flow velocity in its spillway tunnel can reach up to 50 m/s, so a cavitation problem caused by high-velocity flow is prominent. In order to alleviate cavitation damage, aeration devices are employed in the spillway tunnel according to engineering experiences and results of model test [29]. This study aims to use data obtained from a systematic observation of the spillway tunnel to investigate the performance of the aeration system. Together with a series of prototype data from other projects, model scale effect and calculation methods of air demand are discussed, and a new formula to estimate the optimum air demand is also proposed.

## 2. Project Description and Instrumentation

### 2.1. Project Description

The Jinping-I Dam is located on the downstream of the Yalong River in southern China; its location and layout are shown in Figure 1. The total reservoir storage is 7.76 billion m<sup>3</sup>, of which 63% is active. The dam is composed of several discharge structures, including: one controlled spillway with four

gates on its crest, five intermediate orifice openings, two bottom orifice outlets, and one spillway tunnel on the right bank. The maximum discharging capability is 15,400 m<sup>3</sup>/s. Its power station, with an installed capacity of 3600 MW, produces an average annual energy generation of 16.6 billion kW·h. The objective of this project is to supply energy for expanding industrialization and urbanization, improve flood protection, and prevent erosion.

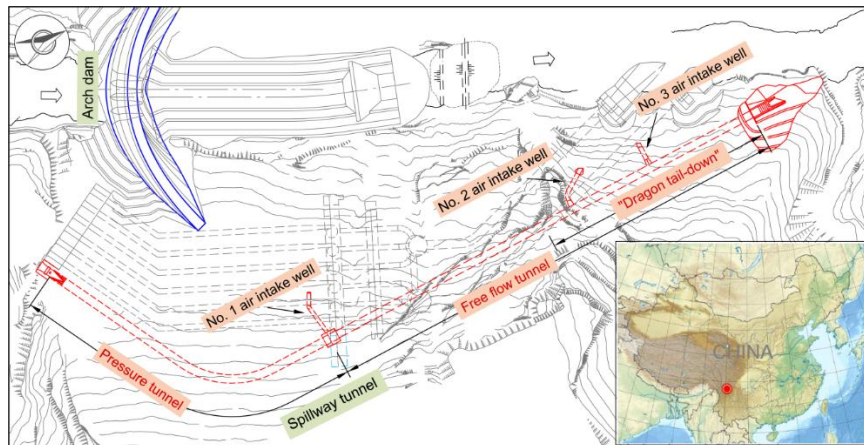


Figure 1. Location and layout of the Jinping-I Dam.

The spillway tunnel is 1407 m long and possesses a structure pattern of “dragon tail-down” in the free flow tunnel (as shown in Figure 1). In order to reduce the length of spillway tunnel with high-velocity flow, 75% of the total head is concentrated in the “dragon tail-down” section, which only accounts for 25% of the total length. The free flow tunnel is with a horse-shaped cross section, the slope angle of its oblique line segment is 24.36°, and the arc radius of its ogee segment is 300 m. A schematic diagram of the free flow tunnel is shown in Figure 2.

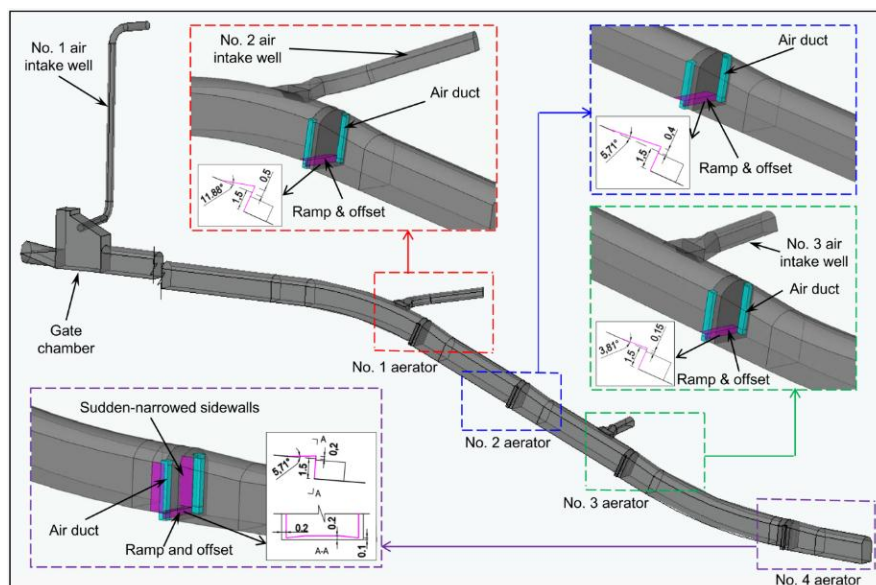


Figure 2. Schematic diagram of the free flow tunnel.

Four aeration devices are employed in the “dragon tail-down” section to prevent cavitation damage (as shown in Figure 2). The first three aerators consist of ramps and offsets, and all of their offsets are 1.5 m high, with the heights of the ramps being 0.5, 0.4, and 0.2 m, respectively.

The fourth aerator is a three-dimensional one, composed of sudden-narrowed sidewalls and convex ramp. Protection lengths of the four aerators are 81.0, 87.8, 128.6, and 115.6 m, respectively. Air ducts connecting to the top of the tunnel are arranged symmetrically on both sides of each aerator. The spillway tunnel of the Jinping-I Dam is constructed inside a mountain, so it is a relatively closed system; three air intake wells for air supply are built. Inlets of the air intake wells are exposed to the atmosphere and outlets of them are set on the roof of the spillway tunnel. The first air intake well is a circular section with a radius of 5.2 m, and the other two air intake wells gradually transform to square sections with the outlet cross section being 9 m wide and 4 m high.

### 2.2. Measurement Points and Instrumentation

Two categories of parameters—the ventilation-related parameters of the air supply system and the aeration-related parameters of the aeration devices—were measured in order to obtain a systematic evaluation on the performance of aeration system in the spillway tunnel. Ventilation-related parameters include average and fluctuating air velocity in the air intake wells and noise caused by air vibration. Aeration-related parameters include air velocity in the air ducts, sub-pressure inside the cavity, air concentration close to the tunnel bottom, cavitation damage depth of the concrete surface, and cavitation noise of the flow. All of measurement points are distributed along the bottom centerline or on sidewalls, and their layouts are shown in Figure 3. The detailed locations of each kind of measurement points are illustrated in Table A1 in Appendix A.

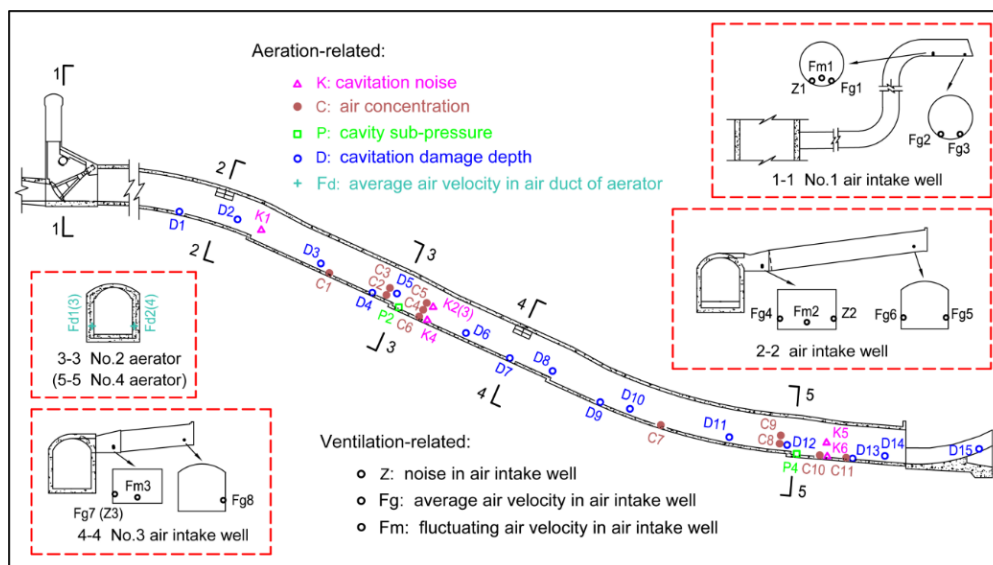
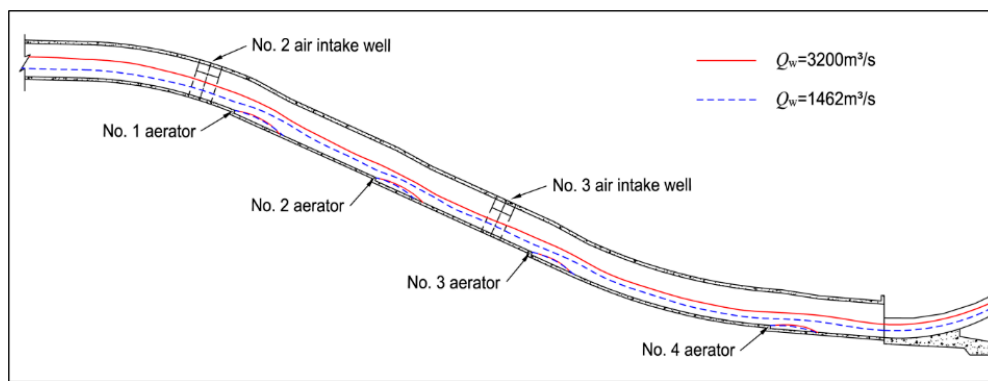


Figure 3. Layout of the measurement points in the prototype.

Field measurements were conducted during the flood season of 2014 and 2015. Parameters for ventilation and aeration at five flow rates—297 m<sup>3</sup>/s, 791 m<sup>3</sup>/s, 1462 m<sup>3</sup>/s, 2130 m<sup>3</sup>/s, and 3200 m<sup>3</sup>/s, corresponding to 8%, 25%, 50%, 75%, and 100% gate opening, respectively, were measured at the design flood level of 1880 m. Surface water profiles in the “dragon tail-down” section of spillway tunnel at typical flow rates are shown in Figure 4 (since it is very difficult to directly measure the surface water profiles in the prototype, the data shown in the figure are obtained from the model test).



**Figure 4.** Surface water profiles in the “dragon tail-down” section of the spillway tunnel at typical flow rates ( $Q_w$ ).

As for the instrumentation used, the air concentration in spillway tunnel was measured via resistance transducers. Average air velocities in both air intake wells and air ducts were measured with a Pitot tube and differential pressure transmitter. Average air velocity can then be calculated from pressure differences by the following formula:

$$V_a = \varphi \sqrt{2g\rho_w / \rho_a \Delta_H} \tag{1}$$

where  $V_a$  is the average air velocity;  $\Delta_H$  is the pressure difference;  $\varphi$  is the Pitot tube coefficient;  $g$  is the gravitational acceleration; and  $\rho_w, \rho_a$  are the density of water and air, respectively. The details of other instrumentations employed in field measurements are given in Table 1.

**Table 1.** Specifications of instrumentations used in prototype observation.

Parameters	Apparatus	Main Technical Specifications
Average air velocity	Pitot tube and differential pressure transmitter	range: 0–126 m/s; accuracy: $\pm 0.5\%$
Air concentration	resistance transducers	range: 0–100%; accuracy: $\pm 0.3\%$
Cavitation noise	hydrophones	working frequency: 1–160 kHz; accuracy: $\pm 3$ dB
Cavity sub-pressure	dynamic pressure transducer	stability: $\pm 0.25\%$ FS; accuracy: $\pm 0.5\%$
Cavitation damage depth	dynamic pressure transducer	stability: $\pm 0.25\%$ FS; accuracy: $\pm 0.5\%$
Fluctuating air velocity	fluctuating anemometer	range: 0–65 m/s; sample frequency: 32 Hz
Noise	Sound level transmitter	range: 0–150 dB resolution ratio: 0.1 dB

### 3. Results

As the spillway tunnel is a relatively closed system, air is sucked into the spillway tunnel through air intake wells. Thereafter, the majority of air is discharged through the water-free space of the spillway tunnel, and only a small amount of air is entrained into the water body by means of cavity artificial aeration and surface self-aeration. As aerated air through cavity aeration experiences a motion trace—firstly, air is sucked into air intake well, then flows past the air duct and enters into the cavity, entrained into the high-velocity water flow finally—the results are also presented in this

order. The results of ventilation-related parameters are elaborated firstly, and then the results of aeration-related parameters.

### 3.1. Ventilation-Related Characteristics of the Air Supply System

The ventilation-related parameters of air supply system include average and fluctuating air velocity in three air intake wells, and noise generated by air vibration.

#### 3.1.1. Average Air Velocity

In the spillway design, air is sucked into the spillway tunnel through the intake wells, and the sizes of the air intake wells are believed to be sufficiently large to ensure adequate air supply where the air velocity is not too high to cause potential damage to the wells. For each air intake well, two measured cross sections were chosen to measure average air velocity. Eight measurement points in total were installed: three each in the No. 1 and No. 2 air intake wells, respectively, and two in the No. 3 air intake well (as shown in Figure 3). Results of the average air velocities at five different flow rates of the spillway are shown in Figure 5.

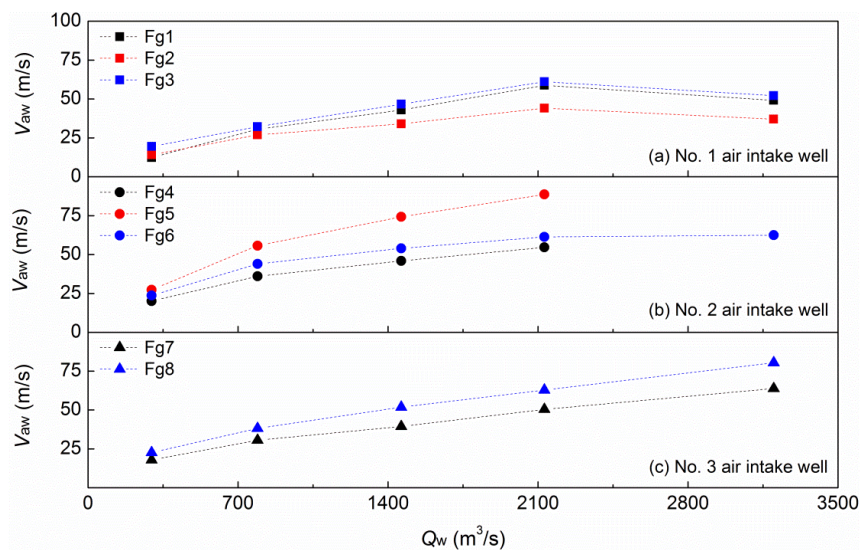


**Figure 5.** Relationship between average air velocity ( $V_{a w}$ ) in the air intake wells and the flow rate in spillway tunnel.

When the flow rate in the spillway tunnel increases from 297 to 3200  $m^3/s$ , average air velocities of the No. 1 to No. 3 air intake wells increase from 12.3 to 61.1 m/s, 20.1 to 88.6 m/s, and 17.9 to 80.4 m/s, respectively, indicating a clear dependency of air velocity on the flow rate. When the flow rate is less than 2130  $m^3/s$ , the increasing trends of air velocities of all air intake wells against the flow rate are consistent. However, when the flow rate is greater than 2130  $m^3/s$ , the trends become inconsistent. With further increasing flow rate, for the No. 1 air intake well the average air velocity slightly decreases, for the No. 2 air intake well it maintains nearly constant, and for the No. 3 air intake well it continues to increase. Restriction from water-free space of spillway tunnel is responsible for the different changing trends. Air is sucked into the spillway tunnel mainly under the action of dragging force imposed by water flow; therefore, greater flow rate generally leads to greater dragging force, then a greater amount of air supply. However, it should be noted that the quantity of air supply is also restricted by cross section size of air intake well and water-free space of the spillway tunnel. When the flow rate is not very large, water depth is relatively shallow. Air quantity through the air intake well is mainly influenced by water flow rate and the air intake well itself, though the influence of the water-free space gradually increases. Thus at flow rates less than 2130  $m^3/s$ , air quantity increases with

increasing flow rate, as do the average air velocities in air intake wells. When the water flow rate is large enough, water depth in some section of the spillway tunnel can become very deep, that is to say, the water-free space may become very narrow. Under these conditions, the air quantity may become mainly restricted by the water-free space. Though greater water flow rate could supply greater driving force, the narrower water-free space may limit the increase of air quantity. The outlets of the No. 1 and No. 2 air intake wells are closer to the upstream, water depths in these positions are more sensitive to water flow rate. When the flow rate is greater than  $2130 \text{ m}^3/\text{s}$ , water depths in these positions become very deep, the narrow water-free space prevents the air quantity from increasing, and the average air velocities in the No. 1 and No. 2 air intake wells do not increase any more. The flow rate has less influence on the water-free space near outlet of the No. 3 air intake well, so the average air velocity in it can continue increasing. The average air velocity in air intake wells increases with increasing flow rate but it may also be affected by water-free space of the spillway tunnel when the flow rate is great enough.

The first measured cross section to measure average air velocity in each air intake well is located near the inlet. The air intake well inlets are all set on the hillside. Affected by the topography boundary, vortices may form near the sidewalls. These vortices would result in non-uniform distribution of the air velocity on the cross section near the inlet. That is why average air velocities of measurement points Fg2 and Fg3 are different though they are symmetrically arranged on the same cross section near the No.1 air intake well inlet, as is the case for measurement points Fg5 and Fg6 in the No. 2 air intake well.

The second measured cross section to measure average air velocity is located at the upper flat section for the No. 1 air intake well, and at the gradually changed section (from the square cross section of 6 m in edge length to the rectangle cross section of 9 m in width and 4 m in height) near the outlet for the No. 2 and No. 3 air intake wells. For the No. 1 air intake well, the two measured cross sections are relatively close. Points Fg1 and Fg3 are at the same position for the two measured cross sections, and their measured values are slightly different. For the No. 2 air intake well, points Fg4 and Fg6 are at the same height on the sidewalls of the two measured cross sections, but their values differ greatly. This is also the case for points Fg7 and Fg8 in the No. 3 air intake well. Inside the air intake well, the average air velocity of cross section is related to the area of cross section according to the continuity equation. For the outlet sections of the No. 2 and No. 3 air intake wells, though the area of two measured cross sections changes little, the airflow at the gradually changed section redistributes due to the impact of the cross section shape, and measured values of the measurement point arranged on sidewalls cannot fully represent the average air velocity of the cross section. Therefore, it is not difficult to understand that differences exist between the average air velocities of measurement points near the outlet (such as points Fg4, Fg7) and those near the inlet (such as points Fg6, Fg8).

### 3.1.2. Fluctuating Air Velocity

Fluctuating air velocity is a parameter to reflect the fluctuation level of air velocity. Three measurement points were set at the cross section center, one for each air intake well. The details of measurement points are shown in Figure 3 and Table A1 (in Appendix A). The data obtained by fluctuating anemometer is instantaneous air velocity, and the difference between the instantaneous air velocity and time-averaged air velocity is fluctuating air velocity.

The amplitude of fluctuating air velocity is randomly distributed, typical time-history curve is shown in Figure 6a; and the fluctuating energy is concentrated in the low frequency domain, mainly within 0–10 Hz (as shown in Figure 6b). The intensity of the fluctuating air velocity is usually expressed as the root mean square (abbreviated as RMS). The RMS of fluctuating air velocity is shown in Figure 6c. The RMS values in the No. 1 air intake well and No. 2 air intake well are in the range of 2.1–5.0 m/s, while the RMS values of No. 3 air intake well are much greater, and the maximum RMS value can reach up to 8.6 m/s. Fluctuation degree of airflow in the air intake well usually is closely related to the turbulence level of water flow. Compared to the No. 1 and No. 2 air intake wells,

the flow velocity near No. 3 air intake well is larger and the turbulence level of water surface is higher. Therefore, the higher turbulence level of water flow in the tunnel leads to a larger fluctuation degree of air velocity in the air intake well.

Time-averaged values obtained from measurement points of fluctuating air velocity are also shown in Figure 6d, and they represent central average air velocity in the air intake wells. The average air velocity obtained from measurement points of average air velocity (as shown in Figure 5) is close to the cross section edge, representing edge average air velocity. For each air intake well, the changing trends of central and edge average air velocity with flow rates are consistent. The central average air velocity is greater than the edge average air velocity for the No. 1 and No. 2 air intake wells, which is reasonable. For the No. 3 air intake well, the velocity of the former is less than that of the latter. This is because a higher turbulence level of water surface can lead to a more uneven level of air flowing out of the air intake well outlet.

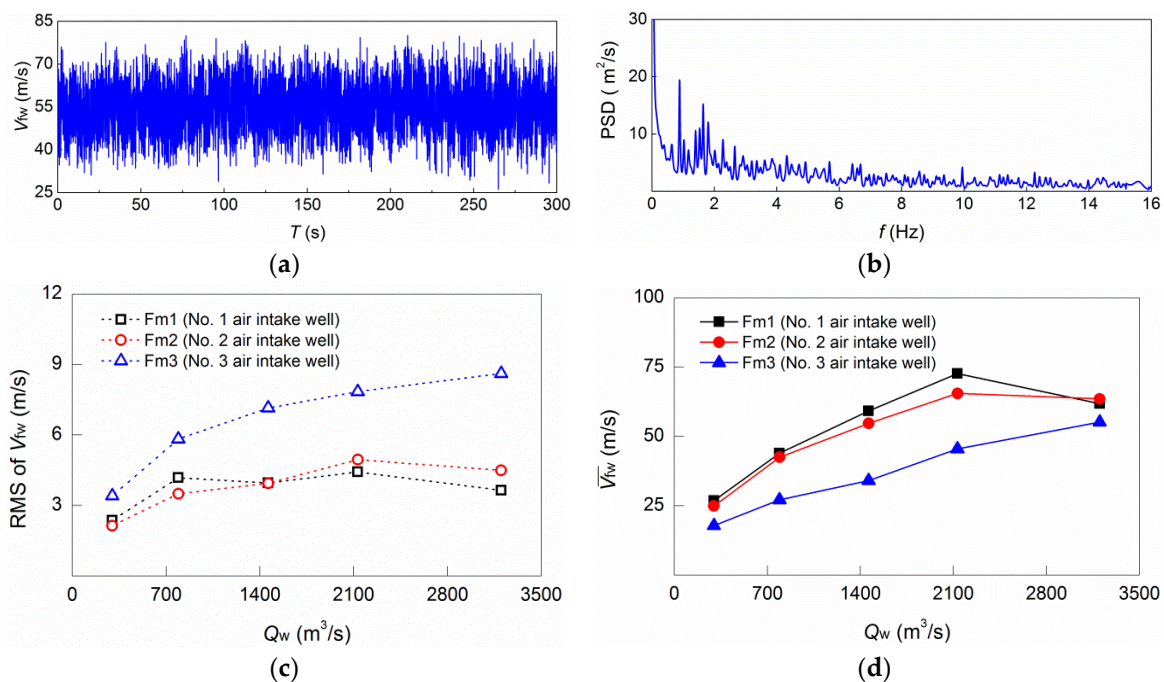


**Figure 6.** (a) Time series of the air velocity fluctuation ( $V_{fw}$ ) measured by point Fm3 at a flow rate of 3200 m<sup>3</sup>/s; (b) power spectral density (PSD) of the velocity fluctuations in (a); (c) root mean square of air velocity fluctuations; (d) time-averaged air velocity ( $\bar{V}_{fw}$ ).

### 3.1.3. Noise

For each air intake well, one noise measurement point was installed: Z1 for the No. 1 air intake well, Z2 for No. 2, and Z3 for No. 3. They were all arranged on the sidewalls near the inlet or outlet of air intake wells. Field measurement results of noise at five different flow rates are shown in Figure 7. The sound pressure level (abbreviated as SPL) in the No. 1–No. 3 air intake wells increases with increasing flow rate as flow rate is less than 2130 m<sup>3</sup>/s; as flow rate further increases, the SPL in the No. 3 air intake well continues increasing, while SPL in the No. 1 air intake well slightly decreases. The dependence of noise on flow rate is exactly similar to that of the air velocity on flow rate. When the flow rate is >791 m<sup>3</sup>/s, all SPLs in air intake wells exceed 100 dB, and the maximum measured value can reach up to 120 dB. As the SPL of noise exceeds 120 dB, there is a risk of hearing loss in cases of prolonged exposure [30]. Such a level of noise can result in noise pollution in the station areas, affecting both the health and behavior of staff working in station, and is therefore cause for attention.

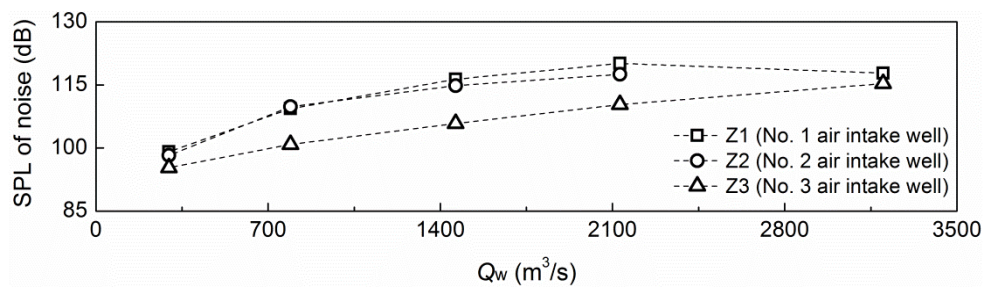


Figure 7. Relationship between the noise generated by air vibration and the flow rate in the spillway tunnel.

### 3.2. Aeration-Related Characteristics of Aeration Devices

The aeration-related parameters of aeration devices mainly include the air velocity in air duct, the sub-pressure inside the cavity, and the air concentration close to the tunnel bottom.

#### 3.2.1. Air Duct Air Velocity and Air Demand

Four aerators were arranged in the spillway tunnel. No. 1, No. 2 and No. 3 are two-dimensional aerators, all located at the oblique-line section. The No. 4 aerator is a three-dimensional aerator located at the end of the ogee segment section. Two typical aerators, No. 2, and No. 4, were chosen to measure air velocity in their air ducts, and results at five different flow rates are shown in Figure 8a.

For the No. 2 aerator, air velocity is from 29.4 to 89.3 m/s for the left air duct, and from 28.5 to 80.0 m/s for the right. For the No. 4 aerator, this value ranges from 25.3 to 79.7 m/s for the left air duct, and 23.9 to 76.4 m/s for the right. Air velocities in left and right air duct are not exactly the same, but the difference is very small, indicating that the airflow evenly flows into the cavity through the left and right air ducts of an aerator. Air velocity in air duct increases with the increase of flow rate, but the growth rate is gradually decreased. When the flow rate is  $>1462$  m<sup>3</sup>/s, air velocities in all air ducts exceed 60 m/s, and the maximum value is close to 90 m/s. The risk of surface damage of air ducts will probably prevail owing to high-velocity airflow [31].

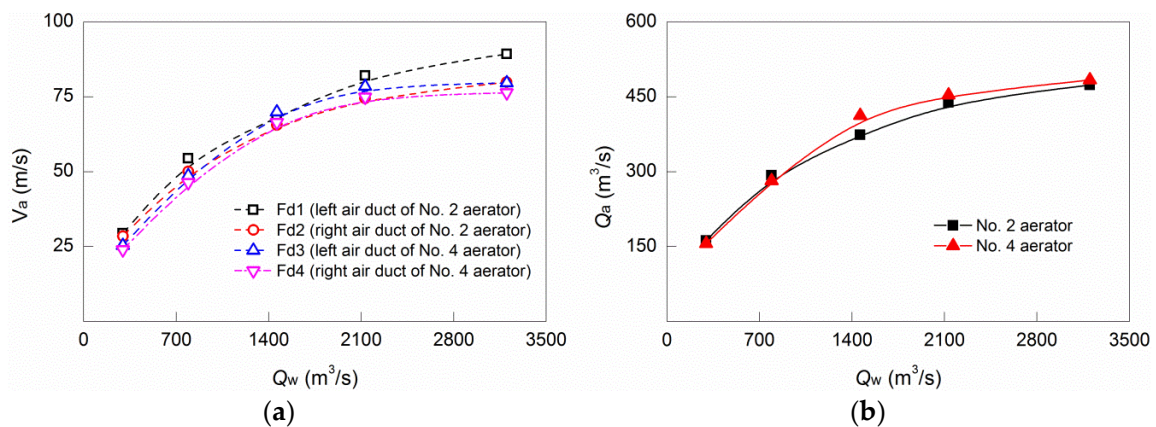


Figure 8. Air velocity ( $V_a$ ) in air ducts (a) and air demand ( $Q_a$ ) of aerators (b) at different flow rates.

Air demand, which is the air quantity supplied by air ducts of aerator, is an important design parameter in terms of the aerator efficiency. It is equal to the average air velocity multiplied by the area of air ducts. Results of air demand are shown in Figure 8b. The changing trend of air demand with flow rate is similar to that of air duct air velocity with flow rate. It increases with increasing flow rate, but the growth trend gradually slows down. With increase of the flow rate, the water depth increases simultaneously, and the turbulence intensity of water flow close to jet lower surface also increases.

As inhibited by water depth, increasing rate of turbulence intensity is not as fast as that of flow rate. Air demand, apart from being influenced by turbulence intensity, is also restricted by the size of air duct, so the increasing rate of air demand is not always a constant value. Varying trends of air velocity in the air duct with flow rate can be explained similarly.

### 3.2.2. Cavity Sub-Pressure

Sub-pressure inside the cavity under the jet is the driving force to pull air into the cavity. The larger the cavity sub-pressure, the greater the amount of air entering from the air ducts. Two measurement points are installed to measure cavity sub-pressure: one (P2) is located at 3.72 m downstream of the No. 2 aerator, and the other (P4) is located at 2.78 m downstream of the No. 4 aerator. At five different flow rates, the two measurement points are not submerged in water, and results of cavity sub-pressure are shown in Figure 9. For the No. 2 aerator, sub-pressure varies from  $-8.26$  kPa to  $-14.25$  kPa. For the No. 4 aerator, it varies from  $-6.26$  kPa to  $-15.77$  kPa. In both aerators, firstly sub-pressure increases with increasing flow rate, and then it almost remains unchanged as flow rate varies from  $1462$  m<sup>3</sup>/s to  $3200$  m<sup>3</sup>/s. The varying trend of cavity sub-pressure with flow rate is similar to that of air demand with flow rate.

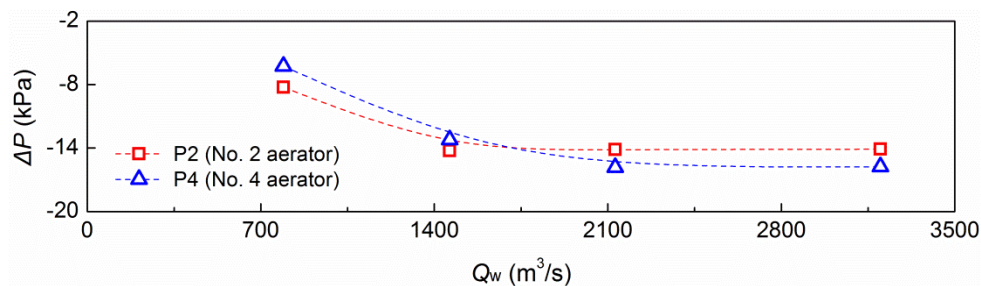


Figure 9. Relationship between cavity sub-pressure ( $\Delta P$ ) and the flow rate in spillway tunnel.

### 3.2.3. Air Concentration

Air concentration is a direct parameter to evaluate aeration effect of water flow. Eleven measurement points were installed to measure air concentration of water flow at different locations, namely: three downstream of No. 1 to No. 3 aerators, and two downstream of No. 4 aerator (as shown in Figure 3). Field results of air concentration at five different flow rates are listed in Table 2.

Table 2. Air concentration (%) along the spillway tunnel at different flow rates.

Series	$Q_w$ (m <sup>3</sup> /s)	No. 1 Aerator Downstream			No. 2 Aerator Downstream			No. 3 Aerator Downstream			No. 4 Aerator Downstream	
		C1	C2	C3	C4	C5	C6	C7	C8	C9	C10	C11
1	297	29.5	37.7	80.82	49.5	85.2	51.7	12.1	79.3	96.9	94.8	60.1
2	791	32.4	12.4	57.9	27.99	71.4	41.3	11.7	6.2	52.3	63.8	42.4
3	1462	31.6	2.8	7.6	20.4	12.0	67.4	11.0	3.9	7.2	70.5	50.4
4	2130	29.2	1.9	3.6	20.7	1.8	68.0	9.4	3.1	5.9	84.4	48.1
5	3200	26.5	1.5	2.9	11.7	0.70	63.7	8.5	2.6	4.0	77.5	27.9

Whether the measurement point is submerged in water or not is related to flow rate. Air concentration of the measurement point can be used to identify its relative position. Generally, air concentration in the air–water interface is 50–60% [32]. If the air concentration of the measurement point is less than 50%, the measurement point is regarded as submerged in water; and if it is greater than 60%, the measurement point is regarded as in cavity or water-free space. As the flow rate increases, water depth in the spillway tunnel increases, then some measurement points on sidewalls may

be gradually submerged in water flow from the water-free space or cavity. Air concentrations of these measurement points correspondingly decrease. According to the above-mentioned criterion, for measurement points located downstream of the No. 1 aerator, C1 and C2 are always submerged in water, and C3 is gradually submerged in water flow as flow rate increases. For measurement points located downstream of the No. 2 aerator, C4 and C5 are gradually submerged in water flow as flow rate increases, and C6 is always upon water flow. For measurement points located downstream of the No. 3 aerator, C7 is always submerged in water, and C8 and C9 are gradually submerged into water from the water-free space. For measurement points located downstream of No. 4 aerator, C10 is always in the cavity considering the relatively high air content, while C11 gradually enters into water from the edge of cavity.

Air concentration at the end of protective range of aerator can be used to determine whether the distance between two aerators is reasonable. The air concentration close to the bottom gradually decreases along the flow direction. When it decays to a small value, another aerator should be set up at that position. C2 and C8 were located on the sidewalls at the end of the protective ranges of the No. 1 and No. 3 aerators, respectively, and they were both 1.1 m away the bottom. The value of C2 is less than 3% when the flow rate is greater than 1462 m<sup>3</sup>/s, and the value of C8 is close to 3% when the flow rate is greater than 2130 m<sup>3</sup>/s. According to a study by Russell [9], such low air concentrations perhaps cannot effectively play a protective role, and the arrangement of the aerator in the spillway tunnel seems to be unsatisfactory. C5 was located on the sidewall near the No. 2 aerator, which is 2.1 m away from the tunnel bottom. When the flow rate is greater than 2130 m<sup>3</sup>/s, its air concentration is less than 3%, indicating that un-airflow area exists on the sidewall. In the cavity area, the self-aeration on jet upper surface and artificial aeration on the jet lower surface both just begin and they have not spread to jet inner. Sidewalls near the aerator may still suffer a risk of cavitation damage; more attention should be paid to protection of this area.

At flow rates of 1462, 2130 and 3200 m<sup>3</sup>/s, according to above analysis, measurement points C1, C2, C7, C8 are all submerged in water flow. Based on the results of these measurement points, attenuation rates of air concentration in the oblique line segment downstream of No. 1 aerator and that in the ogee segment downstream of No. 3 aerator could be obtained, they are ~0.9%/m and ~0.2%/m, respectively (as shown in Table 3), and the attenuation rate decreases slightly with increasing flow rate. According to present observation, attenuation rate of air concentration near the bottom is influenced by the chute slope, and it decreases faster as the slope is greater.

**Table 3.** Attenuation rate of air concentration in the oblique line segment and ogee segment.

Series	Q <sub>w</sub> (m <sup>3</sup> /s)	Oblique Line Segment (C1 to C2)		Ogee Segment (C7 to C8)	
		Distance (m)	Attenuation Rate (%/m)	Distance (m)	Attenuation Rate (%/m)
3	1462	30.74	0.94	65.34	0.23
4	2130	30.74	0.89	65.34	0.21
5	3200	30.74	0.81	65.34	0.19

### 3.3. Effect of Air Entrainment on Cavitation Damage Reduction

In order to evaluate the effect of air entrainment on cavitation damage reduction, the cavitation noise of water flow and damage depth of concrete surface were measured.

Cavitation noise results from sudden collapse of cavitation bubbles. Previous studies have shown that cavitation level and its damage are significantly related to cavitation noise. Measurement of cavitation noise has been proven to be an effective approach in investigation of the cavitation of hydraulic structures [33,34]. In the present observation, six measurement points (as shown in Figure 3) were installed in the spillway tunnel for cavitation noise measurement.

In the process of determining the occurrence of incipient cavitation, the SPL of cavitation noise measured under closed-gate condition is used as the background noise. The SPL amplitude spectrum of

cavitation noise measured by typical measurement point is shown in Figure 10 and the SPL increments of all measurement points are shown in Table 4. As can be seen, the cavitation noise possesses a wide frequency domain, but amplitudes of cavitation noise are relatively concentrated. The SPL increments of measurement points K2, K3, K4 and K5 are small, all less than 2 dB. The SPL increments of point K1 and K6 are relatively large, the maximum values are 18 dB and 9.31 dB, respectively. The measurement point K1 is near the No. 1 aerator, where the flow just begins to be aerated artificially and air concentration of water is small, so its SPL increment is relatively large. Measurement point K6 is located between the points C10 and C11. According to the air concentration results, when the flow rate reaches 2130 m<sup>3</sup>/s, it should be in the vicinity of the air–water interface where the flow is not stable, and the fluctuation of flow causes the SPL to be a bit large. Other measurement points (K2, K3, K4 and K5) are located at the location where the water has been fully aerated, and SPL increments at these measurement points are small. Taking the SPL increment of 6 to 10 dB as the criterion for judging cavitation [35], perhaps the cavitation phenomenon occurs at positions of the measurement points K1 and K6.

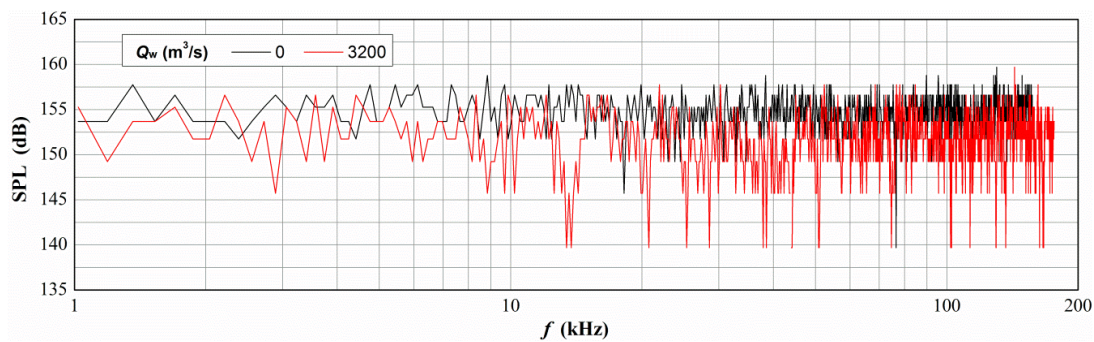


**Figure 10.** Sound pressure level (SPL) amplitude spectrum of cavitation noise measured by measurement point (K1) under closed-gate conditions and at a flow rate of 3200 m<sup>3</sup>/s.

**Table 4.** Sound pressure level (SPL) increment of cavitation noise at different flow rates.

Series	Q <sub>w</sub> (m <sup>3</sup> /s)	Sound Pressure Level (SPL) Increment (dB)					
		K1	K2	K3	K4	K5	K6
2	791	−13.0~9.50	−0.59~0.69	−0.33~0.91	−0.67~0.70	−0.17~0.22	−9.31~0.37
3	1462	−15.5~15.6	−0.72~0.26	−0.59~1.42	−0.92~1.10	−0.22~0.28	−9.29~0.32
4	2130	−18.0~12.0	−0.53~0.38	−0.25~0.68	−0.77~1.77	−0.23~0.32	−8.56~1.12
5	3200	−18.0~13.9	−0.54~0.43	−0.82~0.76	−1.00~0.56	−0.25~0.35	−9.27~0.58

Fifteen measurement points were uniformly arranged on the tunnel bottom or on sidewalls to measure damage depth of concrete surface. Measuring apparatus—dynamic pressure transducers—were buried 5 cm below the concrete surface. If the surface was damaged and stripped to this depth, the transducers could collect the fluid pressure data. The transducer has a full scale of 50 m and an accuracy of 0.5%. At different flow rates, the data collected by the transducers are shown in Figure 11. It can be seen that all the data are within 0.2 m, and not all reach the accuracy of transducers. Such small values indicate that the transducers are not exposed to water, that is, the concrete surfaces around the transducers have not been stripped to the buried depth of transducers and no cracks have extended to this depth.

After two years of flood discharge, on-site inspections were also conducted to check whether any damage occurs on the concrete surface. No obvious traces of damage were observed in the tunnel surface, aeration devices, and air intake wells. This indicates that the layouts of the aeration devices and air intake wells in the Jinping-I Dam spillway tunnel are reasonable.

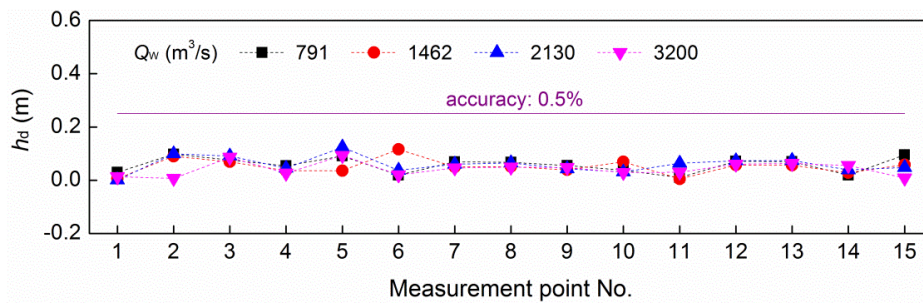


**Figure 11.** Relationship between damage depth ( $h_d$ ) of concrete surface and the flow rate in spillway tunnel.

Although the cavitation phenomenon maybe occurs at some positions, but because of the artificial aeration, the concrete surface is effectively protected from cavitation damage. The fact that low air concentration at the end of protective ranges of No. 1 and No. 3 aerator is also able to effectively prevent cavitation damage, confirms the small bubble theory [8]. As long as the number of air bubble is great enough, low air concentration can also play a protective role.

#### 4. Discussion

Successful application of the aeration device depends on the correct assessment of self-aeration capacity of free jet over the aerator, which generally refers to the air quantity entrained into the flow through the lower surface of free jet, in other words, the air demand of an aerator. Aeration is a complex water–air flow problem, and the air demand is influenced by many factors, such as flow pattern, aeration device type, cavity subpressure, wall roughness, surface tension, water viscosity, and so on.

A typical aeration device is shown in Figure 12, and the aerators’ specific parameters of some projects which have conducted prototype observation are listed in Table A2 in Appendix A.

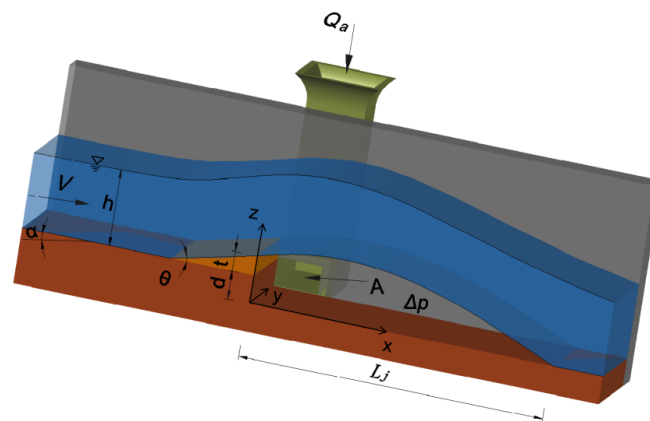


**Figure 12.** Schematic diagram of typical aeration device. Here,  $V$  is the average water velocity;  $h$  is the water depth;  $\alpha$  is the slope angle of the chute;  $d$  is the height of the offset;  $t$  is the height of the ramp;  $\theta$  is the slope angle of the ramp;  $\Delta P$  is the cavity sub-pressure;  $L_j$  is the cavity length;  $A$  is the cross section area of air duct outlet, and  $Q_a$  is the air demand of an aerator. For the coordinate system, the  $x$ -axis is along the water flow direction, the  $y$ -axis is perpendicular to the flow direction, and the  $z$ -axis is perpendicular to the tunnel bottom.

As the air demand is an important parameter in terms of aerator efficiency, the characteristics of air demand, mainly including the similarity between the prototype and the model, and the calculation method, were discussed in this section.

#### 4.1. Model Scale Effect of Air Demand

The physical model of the Jinping-I Dam spillway tunnel is designed according to gravity similarity, and the model scale is  $L_r = 1/30$ . It is a complete model constructed of polymethyl methacrylate. Apparatuses and data acquisition systems employed in the model test are similar to the field measurement. The air demand measured in the model is converted to the prototype by Froude scaling, and the converted prototype air demand is defined as model air demand  $Q_{am}$  (the model air demand is equal to the air demand measured in the model multiplied by  $(1/L_r)^{5/2}$ ).

Prototype and model results of air demand at flow rate of  $3200 \text{ m}^3/\text{s}$  are shown in Figure 13a. Prototype values of the No. 2 aerator and No. 4 aerator are 3.39 and 2.29 times the model values, respectively. Air demand of the aerator in the prototype is considerably greater than that in the model, indicating that the model test designed according to gravity similarity does not obey similarity in air demand. A prototype and model comparison on air concentration is also made (as shown in Figure 13b). For a measurement point completely submerged in the water, owing to more air being entrained in the prototype, the prototype value is much greater than the model values near it, for example in measurement points C1 and C7. For the measurement point completely inside the cavity, since it is exposed to the air, the prototype and model results are similar, for example in measurement points C6 and C10. For the measurement point C11, which is located downstream of the No. 4 aerator, using an air content of 50% to 60% as the criterion for determining the air–water interface, it should be completely submerged in water in the prototype. However, according to the model result, it is inside the cavity. Cavity backwater is more likely to appear in chute with a small bottom slope, and there may be a small amount backwater inside the cavity downstream of the No. 4 aerator in the prototype. The range of the backwater covers C11, but it does not cover C10. The effect of flow aeration in the model test, by contrast, is not as strong as that in the prototype. Therefore, point C11 was inside the cavity in the model test. The significant difference in air concentration between prototype and model also indicates model scale effect exists in model test. Actually, as flow turbulence level is a key factor controlling the amount of air entrained by the flow, un-similarity in turbulence level in model test is mainly responsible for the un-similarity in aeration. If the model scale is greater, the difference in hydraulic parameters including turbulence level between model and prototype could become lesser. The model scale effect on similarity in aeration cannot be neglected.

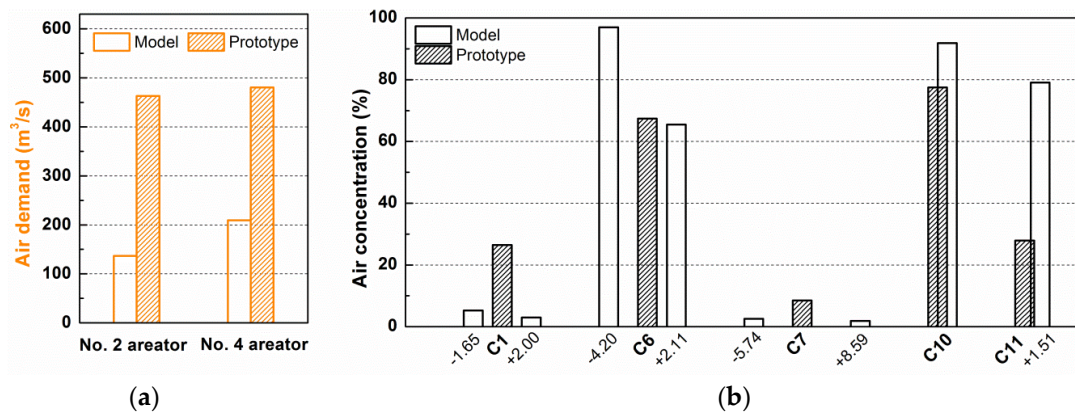


**Figure 13.** Prototype–model comparison of air demand (a) and air concentration (b) at a flow rate of  $3200 \text{ m}^3/\text{s}$ . The positions of model measurement points are listed as distances from their nearest filed measurement points, the negative value indicates the upstream, and the positive value indicates the downstream. The units are in m.

In reality, model scale effect on similarity in aeration could be quantified by air demand ratio between prototype and model air demand ( $n = Q_{ap}/Q_{am}$ ). The closer to one air demand ratio, the less obvious the model scale effect is. Through gathering prototype and model air demand data of many

projects, air demand ratios were calculated. These results, combined with the data of Jinping-I Dam spillway tunnel, are shown in Figure 14 (detailed parameters of aeration devices of these projects are illustrated in Table A2 in Appendix A).

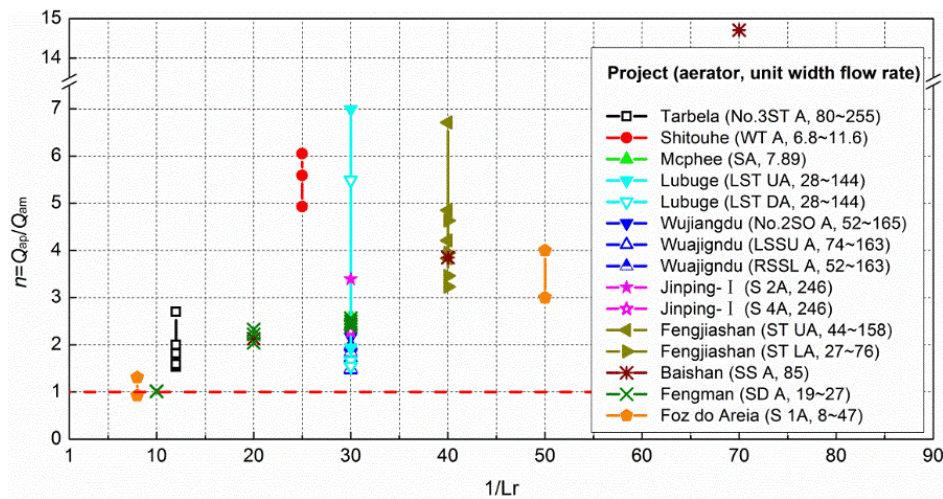


**Figure 14.** Prototype-model air demand ratio versus model scale. The closer to the red dotted line data is, the closer the air demand estimated from the model test is to that in the prototype. Here, the aerator’s location and the unit width flow rate in units of  $m^3/(s \cdot m)$  are described in the parentheses of the legend; for the aerator’s location, the abbreviations before and after the space, respectively, represent the discharge structure and the aerator. The specific meaning of these abbreviations are illustrated in Table A2 in Appendix A.

Model scales range from 1/70 to 1/10, and flow rates range from 8 to 250  $m^3/s$ . For most projects, only one model scale was used. Results of these projects show that the air demand ratio varies with flow rate at a particular model scale, and its sensitivity to flow rate varies from project to project. This is owing to each project having its own characteristics, such as size and type of aerator and slope of the spillway. Pinto and Neidert [22] thoroughly studied the effect of model scale on air demand ratio in the Foz do Areia spillway. Their research showed that the air demand ratio is closer to one as the model scale is greater. Systemic investigations were also conducted in spillways of the Baishan Dam and Fengman Dam by Zhou and Wang [36,37]. Several model scales were used at constant or near constant flow rate. Results of both projects show that air demand ratio decreases with increasing model scale. According to the present available data, although it is difficult to quantify how air demand ratio of a particular spillway aerator is affected by model scale, the tendency that air demand ratio is more likely to be closer to one as model scale used in model test is greater. As proposed by Pinto [18], when the model scale is greater than 1/10, the air demand in model test may be similar to prototype values. However, due to site and economic constraints, the physical model of most projects hardly achieve such a large scale in practice. Model tests according to gravity similarity law could be used to choose the geometries of aeration devices, but the air demand, air concentration and other parameters related to aeration obtained in model tests can only be used as a reference.

#### 4.2. Estimation Method of Air Demand

So far, much research on the calculation method of air demand has been conducted, with most studies involving empirical formulas based on the prototype data. These estimation methods can be roughly classified into two categories.

### 4.2.1. The First Type of Formula

The first type of formula is obtained through theoretical analysis. According to the simplified spray dragging mechanism, the unit width air demand is related to the normal velocity at the jet surface and the cavity length. Supposing the normal velocity is proportional to the axial velocity of the water flow, the general expression of the first type of formula [3,5] is:

$$q_a = KVLj \tag{2}$$

where  $V$  is the axial velocity of water flow;  $Lj$  is the cavity length; and  $K$  is an empirical coefficient. According to the prototype observation results of Foz do Areia, the value of  $K$  is 0.033 for an aerator with air ducts symmetrically arranged on both sides, while it is 0.022 for an aerator with only one duct arranged on one side [5]. According to Equation (2), the value of  $K$  in the Jinping-I spillway tunnel is 0.037 when the unit width flow rate is  $246 \text{ m}^3/(\text{s}\cdot\text{m})$ . The value of  $K$  in the Wujiangdu project is in a wide range, from 0.012 to 0.036. The empirical coefficient  $K$  is not a constant any more. Actually,  $K$  should be a coefficient affected by many factors, such as flow pattern, aerator size and layout, surface roughness, cavity sub-pressure, so it should not be a constant. Considering this fact, Wood [38] has proposed a calculating formula for empirical coefficient, based on the prototype data of Foz do Areia:

$$K = 0.0079(\text{Fr} - 4.3) - 0.16(t/h)(\Delta P/\gamma_w h) \tag{3}$$

where  $\gamma_w$  is the specific weight of water;  $t$  is the ramp height; and  $h$  is the water depth (a typical aeration device and relevant parameters are shown in Figure 12). The value of  $K$  is related to the Froude number  $\text{Fr}$ , aerator ramp height  $t$  and cavity sub-pressure  $\Delta P$ . The effects of offset height and tunnel slope on air demand are not explicitly considered, in addition, cavity sub-pressure is difficult to calculate or estimate in advance; Equation (3) cannot be applicable for all cases.

Though it is difficult to develop a generally applicable expression for  $K$ , the coefficient  $K$  obtained from prototype observations could be used to predict air demand and support design of similar projects in the future. Values of coefficient  $K$  of aerator in some typical projects are listed in Table 5.

**Table 5.** The coefficient  $K$  derived from prototype observation of some projects.

Project	$q_w \text{ (m}^3/\text{s}\cdot\text{m)}$	Aerator			Air Duct	$K$	$\bar{K}$
		Location	$t \text{ (m)}$	$d \text{ (m)}$			
Shitouhe	3.49–31.67	water-conveyance tunnel outlet aerator	0.00	0.35	sym	0.025–0.037	0.034
Baishan	25.50–70.17	surface spillway aerator	0.00	1.66	sym	-	0.024
Jinping-I	112.4–246.1	spillway tunnel No. 2 aerator	0.40	1.50	sym	0.037–0.045	0.041
Fengman	6.53–26.67	spillway dam aerator	0.20	0.00	asym	0.010–0.011	0.010
Guri	6.89–150.0	spillway dam chute 1 lower aerator	0.25	2.84	sym	-	0.026
		spillway dam chute 2 lower aerator	1.50	2.20	sym	-	0.073
Fengjiashan	27.08–76.11	spillway tunnel upper aerator	0.60	0.00	sym	0.019–0.021	0.020
		spillway tunnel lower aerator	0.30	0.00	sym	0.025–0.029	0.028
Foz do Areia	7.58–46.74	spillway No. 1 aerator	0.20	0.00	sym	0.026–0.034	0.030
		spillway No. 2 aerator	0.15	0.00	sym	0.031–0.036	0.033
		spillway No. 3 aerator	0.10	0.00	symmetric	0.026–0.035	0.030
	7.62–29.43	spillway No. 1 aerator	0.20	0.00	asym	0.019–0.021	0.020
		spillway No. 2 aerator	0.15	0.00	asym	0.022–0.030	0.026
Wujiangdu	51.85–163.1	left ski-jump spillway upper aerator	0.61	0.00	asym	0.012–0.015	0.013
		left ski-jump spillway lower aerator	0.85	0.00	sym	0.015–0.021	0.017
	51.85–163.1	right ski-jump spillway lower aerator	0.85	0.00	sym	0.013–0.016	0.015
	52.15–164.6	No.2 spillway opening aerator	0.85	0.00	sym	0.014–0.020	0.015
	38.89–197.8	left spillway tunnel aerator	0.38	0.00	sym	0.012–0.025	0.020
50.33–226.7	right spillway tunnel upper aerator	0.29	0.00	sym	0.033–0.036	0.034	

Notes: ①  $\bar{K}$  is the average value of coefficient  $K$ ; ② “sym” is the abbreviation of symmetric and “asym” is the abbreviation of asymmetric.

#### 4.2.2. The Second Type of Formula

The second type of formula is obtained by means of analyzing the prototype data, establishing the relationship between dimensionless air entrainment rate  $\beta$  (denotes the ratio of unit width air demand to unit width flow rate) with Froude number  $Fr$ , aerator device parameters  $(t, d, \alpha, \theta, \dots)$ , and cavity sub-pressure  $\Delta P$ . The general expression of this type is:

$$\beta = f[Fr, (t, d, \alpha, \theta, \dots), \Delta P] \quad (4)$$

Empirical formulas proposed by Volkart and Rutschmann [39], Bruschin [3], Pinto [26], May et al. [17], Xia [28] and Shi et al. [40], for example, belong to this type of formula. Some of these typical formulas are described below.

The general form of Volkart and Rutschmann [39] formula is:

$$\beta = K_1(Fr - K_2) - K_3 \left( \frac{\Delta P}{\rho gh} \right)^x \quad (5)$$

where  $K_1$ ,  $K_2$  and  $K_3$  are the empirical coefficients depending on the aerator's type, and  $x$  is the empirical index.

With the engineering information of Foz do Areia, Pinto [26] obtained an empirical formula as follows:

$$\beta = 0.47(Fr - 4.5)^{0.59} \left( \frac{C_d A}{Bh} \right)^{0.6} \quad (6)$$

where  $C_d$  is the flow rate coefficient; and  $B$  is the chute width.

The basic type of Shi et al. [40] formula is:

$$\beta = \sqrt{\cos \alpha} (0.00358 + 0.0684X - 0.0387X^{-1}) \quad (7)$$

where  $X$  is a comprehensive hydraulic parameter, related to Froude number, aerator parameters, and water depth. It is expressed as follows:

$$X = Fr \cdot \left( \sqrt{t/h} / \cos \alpha \cdot \cos \theta \right) \quad (8)$$

Compared with the first type formula, the second type formula avoids estimating cavity length in advance, instead applying a Froude number and aerator parameters, so it is more practical. However, the Froude number or water depth should be known by numerical calculation or model tests. Moreover, as each formula is derived from prototype observations of one or several projects, the calculation results of different formulas differ greatly from each other, and this type of formula still lacks universal applicability.

#### 4.2.3. Relationship between Dimensionless Air Entrainment Rate and Unit Width Flow Rate

According to the above-mentioned analysis on air demand formulas, it is still difficult to directly estimate air demand only based on some parameters known in advance, such as aerator parameters and flow rate. Typical prototype observation data on air demand of twelve projects are collected and the profile of dimensionless air entrainment rate  $\beta$  with unit width flow rate  $q_w$  is shown in Figure 15 in log-log coordinates.

For the spillway tunnels of the Jinping-I Dam and the Xiaowan Dam, their discharging capabilities are huge and flow velocities are extremely high; in order to meet the requirements of air entrainment under high velocity conditions, relatively large sizes of aeration devices were employed. As a result, their air entrainment ratios are relatively greater than those of other projects at the same flow rates.

From a group-as-a-whole perspective, the air entrainment rate is inversely proportional to the unit width flow rate, and the changing trend is consistent for different aeration devices. All the curves

roughly follow a power-law relationship. For different aerators, the decreasing rate with flow rate is distinguished, indicating the decreasing rate of dimensionless air entrainment rate is related to aeration devices layout and size. For a particular aerator, the decreasing rate is also not always a constant and it tends to slightly increase with increasing flow rate. In the range of the unit width flow rate  $< \sim 50 \text{ m}^3 / (\text{s} \cdot \text{m})$ , the decreasing rate nearly does not change; while in the range of unit width flow rate  $> \sim 100 \text{ m}^3 / (\text{s} \cdot \text{m})$ , the decreasing rate has a clear growth trend as the unitwidth flow rate increases. This indicates that the decreasing rate of dimensionless air entrainment rate is also related to the unit width flow rate. Therefore, the following formula can be established to relate the dimensionless air entrainment rate with a unit width flow rate:

$$\beta = a \cdot q_w^{b+c(q_w-m)} \tag{9}$$

where a, b, c and m are coefficients, depending on aerator device parameters.

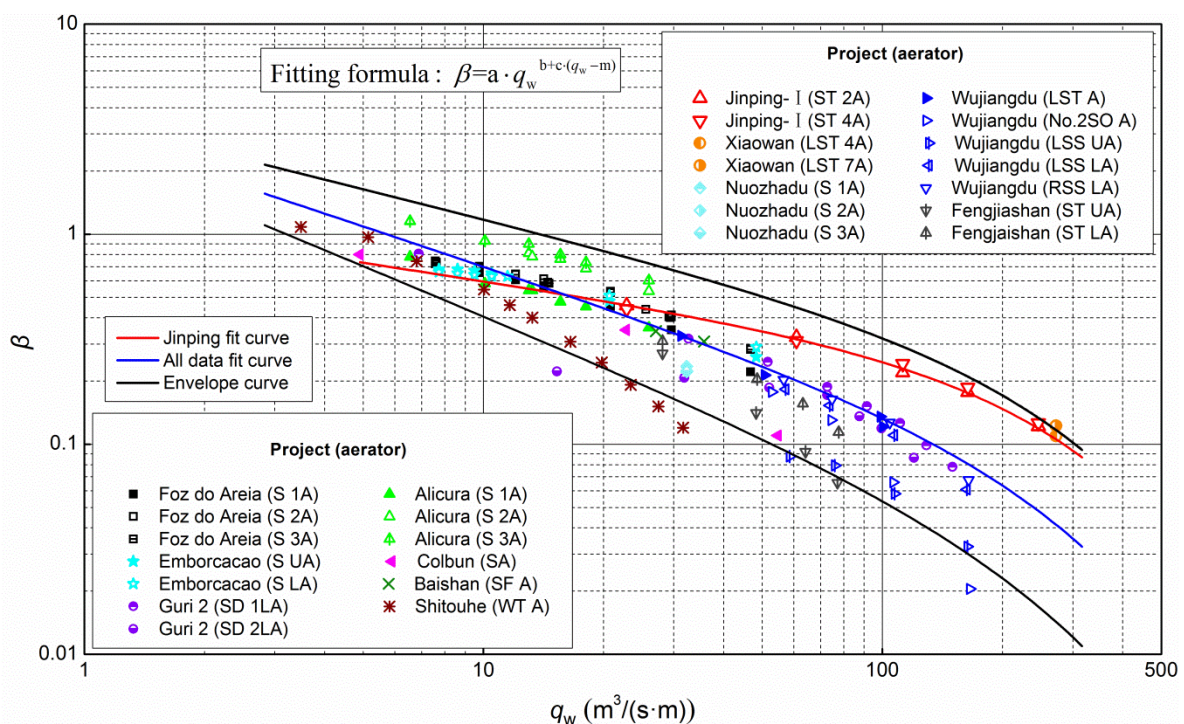


**Figure 15.** Relationship between dimensionless air entrainment rate and the unit-width flow rate in some projects. Here, the aerator’s location is described in the parentheses of the legend, the abbreviations before and after the space, respectively, represent the discharge structure and the aerator. The specific meaning of these abbreviations are illustrated in Table A2 in Appendix A.

By nonlinear least square approximation, values of coefficients a, b, c, m in the Jinping-I spillway tunnel are obtained. They are 1.16, −0.32, −0.0005, and 67.5, respectively. The fitting curve is shown in Figure 15 (the red solid line). As the prototype data are limited, it is unrealistic to definitely establish the relationships of these coefficients with aerator device parameters. By fitting previous prototype data with Equation (9), distribution ranges of coefficient a, b, c, and m can be obtained. For a, it varies from 0.5 to 3.0. For b, it varies from −0.85 to −0.25. For c, it varies from −0.0006 to 0. For m, it varies from 30 to 80. Before drawing a confirm conclusion on how these coefficients vary with aerator parameters, more systemic prototype observations are needed. Apart from being used to establish air demand formula, the collected prototype observation data shown in Figure 15 could also be used as a significant reference for aerator devices design in projects with similar operating conditions.

## 5. Conclusions

In this paper, results of prototype observation on air entrainment performance in the Jinping-I spillway tunnel were presented. Ventilation-related parameters (air velocity in air intake well, air-flow vibration noise) and aeration-related parameters (air velocity in air duct, cavity sub-pressure, air concentration close to tunnel bottom, cavitation damage depth of concrete surface and cavitation noise of flow) at five different flow rates (297, 791, 1462, 2130 and 3200 m<sup>3</sup>/s) were measured.

Generally, air flows smoothly in the air intake wells, but high air velocity and loud noises are observed in some cases. Air velocity in the intake wells is in the range of 12–90 m/s, increasing with the increase of the flow rate in the spillway tunnel, but it may also be affected by spillway tunnel size when the flow rate is large enough. Fluctuating energy of air velocity is mainly concentrated in a low frequency domain (about 0–10 Hz), and its fluctuating intensity is about 5–17% when air is sucked into the air intake well smoothly. The corresponding noise caused by air fluctuation is in the range of 95 to 120 dB, such a level of noise is significant enough to cause instantaneous hearing loss.

The overall effect of air entrainment of the aeration device was regarded as good, as no obvious damage to the concrete bed was found. Air velocity in air duct is in the range of 24–90 m/s, it increases with the increase of the flow rate, with a gradually reduced rate. Cavity sub-pressure varies from −6.26 to −15.77 kPa over the range of flow rates observed, and its dependence on flow rate is similar to that of air velocity. The attenuation rate of air concentration near the bottom is influenced by the chute slope, and is faster as the slope is greater. Relatively low air concentration (less than 3%) at the ends of protective range could also prevent concrete surfaces from cavitation damage. Damage depth of the concrete surface is slight (less than 5 cm), indicating that no significant cavitation occurred after applying aeration devices.

In addition, by comparing the results from the prototype and laboratory experiments, it was found that there is an obvious scale effect on air demand and air concentration distribution. The results showed that only when the model scale is greater than 1/10 can the air demand in the model and prototype be similar. Due to the complexity of the air entrainment phenomenon, the present theoretical formula or empirical formulas for air demand calculation still cannot be universally used in all projects. Moreover, it is found that the air entrainment ratio and unit width flow rate in general follow the power-law. Accordingly, a new formula only related to flow rate and aerator device parameters and used for air demand calculation was established.

To improve the estimation of air demand for the spillway tunnel, further studies should be centered on accurately simulating the flow turbulence level in laboratory model tests, and more systematic prototype observations are also required.

**Acknowledgments:** The authors are grateful to the National Key R&D Program of China (2016YFC0401904), Science Fund for Innovative Research Groups of the National Natural Science Foundation of China (51621092), Program of Introducing Talents of Discipline to Universities (B14012), Tianjin Research Program of Application Foundation and Advanced Technology (15JCQNJC07100) and the Tianjin Innovation Team Foundation of Key Research Areas (2014TDA001) for financial support. Additionally, the authors thank the China Institute of Water Resources and Hydropower Research for experimental support. Finally, the authors would like to express their sincere gratitude to all of those who have offered selfless help during the course of this research.

**Author Contributions:** All authors (Jijian Lian, Chunfeng Qi, Fang Liu, Wenjuan Gou, Shunqi Pan, Qunan Ouyang) contributed to the research work. Jijian Lian, Fang Liu and Wenjuan Gou conceived and designed the prototype observation; Chunfeng Qi and Qunan Ouyang performed the prototype tests and analyzed the data; Shunqi Pan contributed analysis tools; and Chunfeng Qi drafted the paper.

**Conflicts of Interest:** The authors declare no conflict of interest.

Appendix A

**Table A1.** Measurement point details of ventilation-related and aeration-related parameters in the prototype.

Parameter	Point Name	Location	Vdb (m)	Parameter	Point Name	Location	Vdb (m)
Average air velocity at cross section edge of air intake well	Fg1	No. 1 right sidewall	0.4	Damage depth of concrete surface inside spillway tunnel	D1	bottom centerline	0
	Fg2	No. 1 left sidewall	0.4		D2	left sidewall	5.0
	Fg3	No. 1 right sidewall	0.4		D3	left sidewall	3.0
	Fg4	No. 2 left sidewall	1.4		D4	bottom centerline	0
	Fg5	No. 2 right sidewall	1.4		D5	left sidewall	3.0
	Fg6	No. 2 left sidewall	1.4		D6	left sidewall	3.0
	Fg7	No. 3 left sidewall	1.4		D7	bottom centerline	0
	Fg8	No. 3 right sidewall	1.4		D8	left sidewall	3.0
Fluctuating air velocity at cross section center of air intake well	Fm1	No. 1	0.9		D9	bottom centerline	0
	Fm2	No. 2	0.9		D10	left sidewall	3.0
	Fm3	No. 3	0.9		D11	left sidewall	3.0
Noise at cross section edge of air intake well	Z1	No. 1 left sidewall	0.4		D12	left sidewall	3.0
	Z2	No. 2 right sidewall	1.4		D13	bottom centerline	0
	Z3	No. 3 left sidewall	1.4		D14	left sidewall	3.0
Average air velocity in air duct of aerator	Fd1	No. 2 left sidewall	3.5		D15	left sidewall	1.0
	Fd2	No. 2 right sidewall	3.5	C1	bottom centerline	0	
	Fd3	No.4 left sidewall	3.5	C2	left sidewall	1.1	
	Fd4	No. 4 right sidewall	3.5	C3	right sidewall	2.1	
Sub-pressure inside cavity of aerator	P2	downstream No. 2	0	Air concentration close to bottom inside spillway tunnel	C4	left sidewall	1.1
	P4	downstream No. 4	0		C5	right sidewall	2.1
Cavitation noise of water flow inside spillway tunnel	K1	left sidewall	2.1		C6	bottom centerline	0
	K2	left sidewall	3.1		C7	bottom centerline	0
	K3	right sidewall	2.1		C8	left sidewall	1.1
	K4	bottom centerline	0		C9	right sidewall	2.1
	K5	right sidewall	2.1		C10	bottom centerline	0
	K6	bottom centerline	0		C11	bottom centerline	0

Note: Vdb refers to the vertical distance of the measurement point from the bottom.

**Table A2.** Specific parameters of aeration devices in some projects conducted with prototype observation.

Project (Country)	Aerator						A (Number, Shape, Size (m))
	Location (Abbreviation)	$\alpha$ (°)	$\theta$ (°)	$t$ (m)	$d$ (m)		
Alicura (Argentina)	spillway aerator (S A)	19.29	9.90	0.175	0.00	2□3 × 1.02	
Baishan (China)	surface spillway aerator (SS A)	63.40	0.00	0.00	1.66	2Φ1.2	
Colbun (Chile)	spillway aerator (S A)	27.10	11.30	0.25	0.00	2□3 × 1.5	
Fengman (China)	spillway dam aerator (SP A)	52.00	11.30	0.20	0.00	1□0.3 × 0.5	
Libby (America)	sluiceway aerator (SA)	17.50	3.18	0.04	0.00	2 × 1.49	
Longyangxia (China)	intermediate orifice opening aerator (IO A)	15.00	5.71	0.50	0.00	2Φ1.0	
McPhee (America)	spillway aerator (S A)	18.40	6.40	0.90	0.00	2□0.91 × 1.22	
Tarbela (Pakistan)	No.3 spillway tunnel aerator (No.3ST A)	0.00	7.13	0.14	0.00	2Φ1.0	
Dongjiang (China)	ski-jump spillway upper aerator (SS UA)	43.85	2.86	0.40	0.60	2Φ1.0	
	ski-jump spillway lower aerator (SS LA)	32.73	5.71	0.30	0.60	2Φ1.0	
Emborcaao (Brazil)	spillway upper aerator (S UA)	10.20	7.13	0.30	0.00	2□4.2 × 1.5	
	spillway lower aerator (S LA)	10.20	7.13	0.20	0.00	2□4.2 × 1.5	
Fengjiashan (China)	spillway tunnel upper aerator (ST UA)	26.56	3.81	0.60	0.00	2Φ0.9	
	spillway tunnel lower aerator (ST LA)	0.13	7.13	0.30	0.00	2Φ0.9	
Three Gorges (China)	spillway dam aerator (SD A)	55.00	11.30	0.80	0.00	2Φ1.3	
	bottom orifice outlet aerator (BO A)	0.00	0.00	0.00	1.50	2Φ1.4	
Guri 2 (Venezuela)	spillway dam chute 1 lower aerator (SD 1LA)	51.30	5.00	0.25	2.84	6□1.25 × 1.25	
	spillway dam chute 2 lower aerator (SD 2LA)	51.30	25.00	1.50	2.20	6□1.25 × 1.25	

Table A2. Cont.

Project (Country)	Location (Abbreviation)	Aerator				A (Number, Shape, Size (m))
		$\alpha$ (°)	$\theta$ (°)	$t$ (m)	$d$ (m)	
Foz do Areia (Brazil)	spillway No. 1 aerator (S 1A)	14.49	7.13	0.20	0.00	2□4 × 1.8
	spillway No. 2 aerator (S 2A)	14.49	7.13	0.15	0.00	2□4 × 1.8
	spillway No. 3 aerator (S 3A)	14.49	7.13	0.10	0.00	2□4 × 1.8
Shitouhe (China)	spillway tunnel upper aerator (ST UA)	21.80	5.76	0.15	0.00	2□0.64 × 1
	spillway tunnel lower aerator (ST LA)	0.57	5.76	0.15	0.00	2□0.64 × 1
	water-conveyance tunnel outlet aerator (WT A)	3.58	0.00	0.00	0.35	2□0.25 × 1
Lubuge (China)	left spillway tunnel upper aerator (LST UA)	7.09	7.13	0.80	0.00	2□2.5 × 0.8
	left spillway tunnel lower aerator (LST LA)	0.22	7.13	0.60	0.00	2□2.0 × 0.6
	left spillway upper aerator (LS UA)	18.26	11.30	0.80	0.80	1□0.65 × 1.95 + 1□0.5 × 2
	left spillway lower aerator (LS LA)	18.26	11.30	0.40	0.80	1□0.56 × 1.70 + 1□0.5 × 2
Jinping-I (China)	spillway tunnel No. 1 aerator (ST 1A)	24.36	11.88	0.50	1.50	2□1.8 × 1.2
	spillway tunnel No. 2 aerator (ST 2A)	24.36	5.71	0.40	1.50	2□2.0 × 1.4
	spillway tunnel No. 3 aerator (ST 3A)	24.36	3.81	0.15	1.50	2□2.0 × 1.4
	spillway tunnel No. 4 aerator (ST 4A)	4.57	5.71	0.20	1.50	2□2.2 × 1.4
Nuozhadu (China)	spillway No. 1 aerator (S 1A)	0.76	5.72	0.30	3.50	2□4 × 3.46
	spillway No. 2 aerator (S 2A)	12.95	7.95	0.80	4.00	2□4 × 3
	spillway No. 3 aerator (S 3A)	12.95	7.95	0.60	4.00	2□4 × 3
	spillway No. 4 aerator (S 4A)	12.95	5.69	0.60	4.00	2□4 × 3
	spillway No. 5 aerator (S 5A)	12.95	5.69	0.50	4.00	2□4 × 3
Wujiangdu (China)	left ski-jump spillway upper aerator (LSS UA)	54.14	4.84	0.61	0.00	2Φ1.2
	left ski-jump spillway lower aerator (LSS LA)	19.26	11.30	0.85	0.00	2Φ1.2
	right ski-jump spillway lower aerator (RSS LA)	19.26	11.30	0.85	0.00	2Φ1.2
	No.2 spillway opening aerator (No.2SO A)	55.02	11.30	0.85	0.00	2Φ1.2
	left spillway tunnel aerator (LST A)	33.69	3.28	0.38	0.00	4Φ1.2
	right spillway tunnel upper aerator (RST UA)	19.20	12.60	0.29	0.00	2□1.2 × 2
right spillway tunnel lower aerator (RST LA)	2.70	0.00	0.00	1.00	2□0.85 × 2.5	
Xiaowan (China)	left spillway tunnel No. 1 aerator (LST 1A)	23.69	5.71	0.53	1.30	2□2.5 × 1.5
	left spillway tunnel No. 2 aerator (LST 2A)	2.41	0.00	0.00	2.50	2□2.5 × 1.5
	left spillway tunnel No. 3 aerator (LST 3A)	6.03	0.00	0.00	2.00	2□2.5 × 1.5
	left spillway tunnel No. 4 aerator (LST 4A)	6.03	0.00	0.00	2.00	2□2.5 × 1.5
	left spillway tunnel No. 5 aerator (LST 5A)	6.03	0.00	0.00	2.00	2□2.5 × 1.5
	left spillway tunnel No. 6 aerator (LST 6A)	6.03	0.00	0.00	2.00	2□2.5 × 1.5
	left spillway tunnel No. 7 aerator (LST 7A)	6.03	0.00	0.00	2.00	2□2.5 × 1.5

Notes: ① “□” represents a rectangular cross section, and the numbers after it represent the length and width;  
 ② “Φ” represents a circular cross section, and the number after it represents the diameter.

## References

- Chanson, H. Flow downstream of an aerator-aerator spacing. *J. Hydraul. Res.* **1989**, *27*, 519–536. [CrossRef]
- Rutschmann, P.; Hager, W.H. Air entrainment by spillway aerators. *J. Hydraul. Eng.* **1990**, *116*, 765–782. [CrossRef]
- Bruschin, J. Forced aeration of high velocity flows. *J. Hydraul. Res.* **1987**, *25*, 5–14. [CrossRef]
- Pfister, M.; Hager, W.H. Chute aerators. I: Air transport characteristics. *J. Hydraul. Eng.* **2010**, *136*, 352–359. [CrossRef]
- Pinto, N.L.S.; Neidert, S.; Ota, J. Aeration at high velocity flows. *Int. Water Power Dam Constr.* **1982**, *34*, 34–38.
- Kells, J.A.; Smith, C.D. Reduction of cavitation on spillways by induced air entrainment. *Can. J. Civ. Eng.* **1992**, *19*, 928–929. [CrossRef]
- Peterka, A.J. The effect of entrained air on cavitation pitting. In Proceedings of the Minnesota International Hydraulic Convention, Minneapolis, MN, USA, 1–4 September 1953; pp. 507–518.
- Rasmussen, R. Some experiments on cavitation erosion in water mixed with air. In *International Symposium on Cavitation in Hydrodynamics*; National Physical Laboratory: London, UK, 1956; pp. 1–25.
- Kramer, K.; Hager, W.H.; Minor, H.E. Development of air concentration on chute spillways. *J. Hydraul. Eng.* **2006**, *132*, 908–915. [CrossRef]
- Ball, J.W. Cavitation from surface irregularities in high velocity. *J. Hydraul. Div.* **1976**, *102*, 1283–1297.
- Hamilton, W. Preventing cavitation damage to hydraulic structures; part three. *Int. Water Power Dam Constr.* **1984**, *36*, 42–45.
- Wood, I.R. Uniform region of self-aerated flow. *J. Hydraul. Eng.* **1983**, *109*, 447–461. [CrossRef]
- Elder, R.A. Advances in hydraulic engineering practice: The last four decades and beyond. *J. Hydraul. Eng.* **1986**, *112*, 73–89. [CrossRef]

14. Falvey, H.T. *Cavitation in Chutes and Spillways*, 1st ed.; United States Department of the Interior: Denver, CO, USA, 1990.
15. Pan, S.-B.; Shao, Y.-Y.; Shi, Q.-S.; Dong, X.-L. The self-Aeration Capacity of the Water Jet over the Aeration Ramp. *Shuili Xuebao* **1980**, *5*, 13–22. (In Chinese)
16. Koschitzky, H.P.; Kobus, H. Hydraulics and design of spillway aerators for cavitation prevention in high speed flows. In Proceedings of the International Symposium on Hydraulic for High Dams, Beijing, China, 15–18 November 1988; pp. 724–733.
17. May, R.; Escarameia, M.; Karavokyris, I. Scaling the performance of aerators in a tunnel spillway. In Proceedings of the 26th Congress of the International Association for Hydraulic Research, London, UK, 11–15 September 1995; pp. 444–449.
18. Chen, C.-Z.; Yu, Q.-Y. Air Entrainment characteristics of flow over an aerator device with ramp. *Water Resour. Hydropower Eng.* **1999**, *30*, 26–30. (In Chinese)
19. Haberman, W.L.; Morton, R.K. An experimental study of bubbles moving in liquids. *Trans. Am. Soc. Civ. Eng.* **1954**, *121*, 227–250.
20. Domgin, J.; Gardin, P.; Brunet, M. Experimental and numerical investigation of gas stirred ladles. In Proceedings of the Second International Conference on CFD in the Minerals and Process Industries CSIRO, Melbourne, Australia, 6–8 December 1999; pp. 181–196.
21. Volkart, P. Transition from aerated supercritical to subcritical flow and associated bubble de-aeration. In Proceedings of the 21st Congress of the International Association for Hydraulic Research, Melbourne, Australia, 19–23 August 1985; pp. 2–6.
22. Pinto, N.L.S.; Neidert, S.H. Model prototype conformity in aerated spillway flow. In Proceedings of the International Conference on the Hydraulic Modelling of Civil Engineering Structures, Coventry, UK, 22–24 September 1982; pp. 22–24.
23. Chanson, H. Air-water flows in water engineering and hydraulic structures basic processes and metrology. In *Hydraulics of Dams & River Structures, Proceedings of the International Conference on Hydraulics of Dams and River Structures, Tehran, Iran, 26–28 April 2004*; Yazdandoost, Y., Attari, J., Eds.; A.A.Balkenma Publishers: Tehran, Iran, 2004; pp. 3–16.
24. Frizell, K.W. Glen Canyon Dam Spillway Tests Model-Prototype Comparison. Available online: <http://cedb.asce.org/CEDBsearch/record.jsp?dockkey=0045955> (accessed on 10 September 2017).
25. Nemesio, C.R.; Marcano, A. Aeration at guri final stage spillway. In Proceedings of the International Symposium on Model-Prototype Correlation of Hydraulic Structures, Colorado, CO, USA, 9–11 August 1988; pp. 102–109.
26. Pinto, N.D.S. Designing aerators for high velocity flow. *Int. Water Power Dam Constr.* **1989**, *41*, 44–48.
27. Semenov, V.; Lentyaev, L. Spillway with nappe aeration. *Power Technol. Eng.* **1973**, *7*, 436–441. [[CrossRef](#)]
28. Xia, Y.-P. An analysis of prototype observation for air entrainment of aerations devices on Wujiangdu and Fengjiashan hydraulic structures. *Shuili Xuebao* **1990**, *2*, 37–41. (In Chinese)
29. Wu, Y.-H. Experiment study on hydraulic model of spillway tunnel at Jinping-I Dam. Unpublished.
30. Roeser, R.J.; Valente, M. *Audiology-Diagnosis*, 2nd ed.; Thieme Publishing Group: New York, NY, USA, 2007; p. 240.
31. Water Resources Department of the People's Republic of China. *SL253–2000 Design Code for Spillway*; China Water Conservancy and Hydropower Press: Beijing, China, 2000; p. 71.
32. Straub, L.G.; Lamb, O.P. Experimental studies of air entrainment in open channel flow. In Proceedings of the Minnesota International Hydraulic Convention, Minneapolis, MN, USA, 1–4 September 1953; pp. 425–437.
33. Lush, P.; Angell, B. Correlation of cavitation erosion and sound pressure level. *J. Fluid. Eng.* **1984**, *106*, 347–351. [[CrossRef](#)]
34. Zhang, D.; Liu, Z.-P.; Jin, T.-L.; Xiang, Y.-P. Cavitation inception witnessed by sound pressure level in model test and prototype observation. *J. Hydrodyn. Ser. B* **2004**, *16*, 227–232.
35. Wu, J.-H.; Wu, W.-W.; RUAN, S.-P. On necessity of placing an aerator in the bottom discharge tunnel at the longtan hydropower station. *J. Hydrodyn. Ser. B* **2006**, *18*, 698–701. [[CrossRef](#)]
36. Zhou, L.; Wang, J. Erosion damage at fengman spillway dam and investigation on measures of preventing cavitation. In Proceedings of the International Symposium on Hydraulics for High Dams, Beijing, China, 15–18 November 1988; pp. 703–709.
37. Zhou, L.-P.; Wang, J.-P. Experiment study and prototype observation of aeration devices in surface spillway of Baishan arch dam. *Water Resour. Hydropower Eng.* **1988**, *1*, 2–6. (In Chinese)

38. Wood, I. Air water flows. In Proceedings of the 21st Congress of the International Association for Hydraulic Research, Melbourne, Australia, 19–23 August 1985; pp. 18–29.
39. Volkart, P.; Rutschmann, P. Aerators on Spillway Chutes: Fundamentals and Applications. Available online: <http://cedb.asce.org/CEDBsearch/record.jsp?dockey=0048612> (accessed on 10 September 2017).
40. Shi, Q.-S.; Pan, S.-B.; Shao, Y.-Y.; Yuan, X. Experimental investigation of flow aeration to prevent cavitation erosion by a deflector. *J. Hydraul. Eng.* **1983**, *3*, 1–13.



© 2017 by the authors. Licensee MDPI, Basel, Switzerland. This article is an open access article distributed under the terms and conditions of the Creative Commons Attribution (CC BY) license (<http://creativecommons.org/licenses/by/4.0/>).